

Interplay of Electron-Magnon Scattering and Spin-Orbit Induced Electronic Spin-Flip Scattering in a two-band Stoner model

Felix Dusabirane,^{1,2,*} Kai Leckron,¹ Baerbel Rethfeld,¹ and Hans Christian Schneider^{1,†}

¹*Physics Department and Research Center OPTIMAS,
University of Kaiserslautern-Landau, P.O. Box 3049, 67663 Kaiserslautern, Germany*

²*Department of Physics, College of Science and Technology,
University of Rwanda, P.O. Box 3900, Kigali, Rwanda.*

This paper presents a theoretical investigation of the influence of electron-magnon scattering processes on the ultrafast demagnetization in itinerant ferromagnets. In the framework of a ferromagnetic model system, we compute the spin-dependent dynamics of electrons in itinerant Bloch states including electron-magnon and electron-electron scattering. Our approach includes both electron-magnon and electron-electron scattering processes on an equal footing. While the former process flips the electronic spin accompanied by the creation or destruction of a magnons, the latter exchanges electronic angular momentum with the lattice due to the influence of spin-orbit coupling. We show that the *interplay* of the two different scattering mechanisms leads to the creation of magnons and a transfer of angular momentum to the lattice that, for a realistic choice of the electron-magnon interaction and excitation conditions, is considerably more efficient than spin-orbit assisted electron-electron scattering alone. This process of magnon creation and spin-lattice coupling constitutes an essentially non-equilibrium microscopic scenario for the ultrafast demagnetization process in itinerant ferromagnets.

I. INTRODUCTION

The discovery of optically induced ultrafast demagnetization in metallic ferromagnets [1] has led to the question how the spin angular momentum of the electrons is dissipated on a 100 fs timescale. Different proposals exist, which all involve spin-orbit coupling in one way or another. Early on, it was suggested that a mechanism of the Elliott-Yafet (EY) type could be responsible for the angular momentum dissipation, either to phonons or to the lattice [2–4]. In this mechanism, it is the combination of spin-orbit coupling and the electron-phonon scattering process which dissipates the angular momentum. Importantly, the interaction of electrons with longitudinal phonons is predominantly spin independent, whereas the explicitly spin dependent contribution is extremely small in ferromagnets [5–7] and mainly important in materials with spin degenerate bands, such as semiconductors and simple metals [8–12]. In the case of spin-split bands, the spin independent electron-phonon interactions leads essentially to incoherent electronic spin-flip transitions due to spin-orbit coupling in the Bloch states that underlies the Elliott-Yafet mechanisms, as was shown, for instance, in Ref. [13] for an extension of the Elliott-Yafet mechanism that also includes spin coherences and their dephasing. For the purposes of this paper we will describe electronic transitions that change the electronic spin due to spin-orbit coupling as incoherent scattering processes. In particular, we use this approach, which computes the dynamical changes of the electronic distributions at the level of Boltzmann scattering integrals [14, 15], for

electron-electron Coulomb scattering. However, we do not consider the direct influence of the coherent electromagnetic field on the electronic orbital degree of freedom [16, 17] nor that of polarized phonons [18].

The main purpose of this paper is to study how electron-magnon scattering processes affect ultrafast demagnetization, in particular as they compete with other scattering mechanisms such as electron-electron and electron-phonon scattering that lead to an angular momentum exchange with the lattice. The importance of magnons for demagnetization was stressed early on [19–23]. Most importantly for the present paper, the calculation of separate electron-phonon and electron-magnon transitions rates [24] was used to suggest the interplay of the two processes as a candidate process for ultrafast demagnetization more than a decade ago. Recently, the magnon contribution to demagnetization has received renewed attention. For instance, the interaction of electrons with magnons and spin-orbit assisted EY-spin-flips has been included in the derivation of macroscopic transport equations for ferromagnet-heterostructures [25, 26], and a $(N + 2)$ -temperature model for mode-resolved magnon temperatures has been introduced [27].

We explore the coupled electron and magnon *dynamics* during the demagnetization process in a model ferromagnet with the focus on electronic and magnonic non-equilibrium effects. We therefore avoid the assumption of exact Fermi-Dirac distributions for the itinerant electrons of the ferromagnet, which underlies Refs. [25, 27]. Our approach is suitable to describe the interplay of the two scattering mechanisms, which is particularly important away from equilibrium during the early stages of the demagnetization process.

In order to study the non-equilibrium electron-magnon dynamics we employ a microscopic model that includes electron-magnon interactions and spin-orbit as-

* f.dusabirane@ur.ac.rw

† hc.schneider@rptu.de

sisted spin-flip electron-electron scattering processes. From the calculation of the interacting electron and magnon dynamics we show how the loss of magnetization at short times arises as a non-equilibrium process due to the interplay of the different electronic scattering mechanisms. Furthermore, we argue that an additional relaxation mechanism for the magnons is needed in order to describe the remagnetization process.

The paper is organized as follows. In Sec. II we describe our model of electrons, magnons and their interactions in a band structure with two Stoner spin-split bands and spin-orbit contributions in the wave functions. We set up the dynamical equations for the distribution functions of electrons and magnons including the relevant scattering mechanisms. In Sec. III we calculate results for the dynamics of the distribution functions after an instantaneous excitation process. We show that magnons at high energies and q vectors are created in a process that involves magnon-emission processes and highlight the impact of EY-like spin-flip scattering of the electrons. We also show the importance of different relaxation processes for the remagnetization dynamics and present our conclusions in Sec. IV.

II. MODEL AND DYNAMICAL EQUATIONS

A. Basic Hamiltonian

In this section, we set up a model and describe our theoretical approach to calculate ultrafast spin dependent electronic dynamics due to electron-magnon, electron-electron and electron-phonon interactions.

Electrons, magnons and phonons are governed by the following general Hamiltonian

$$H = H_e + H_m + H_p + V_{e-e} + V_{e-m} + V_{e-p} + V_{m-p} \quad (1)$$

which includes the electron-electron Coulomb interaction, the electron-magnon interaction, the electron-phonon interaction and magnon-phonon interactions, respectively. We will treat the first two of these interactions dynamically and the latter two using relaxation-time approximations in the present paper. The first term describes the single-electron contribution in our model

$$H_e = \sum_{\mathbf{k}, \sigma} \epsilon_{\mathbf{k}, \sigma} c_{\mathbf{k}, \sigma}^\dagger c_{\mathbf{k}, \sigma} \quad (2)$$

where we have denoted by $c_{\mathbf{k}, \sigma}^\dagger$ ($c_{\mathbf{k}, \sigma}$) the creation (annihilation) operators for electrons with crystal momentum \mathbf{k} and spin σ . The single-electron Hamiltonian may include self-energy effects such as a *dynamical* spin splitting. An explicit form for the energy will be given in Sec. II E further below. An extension to the multi-band case is straightforward, but would enormously complicate the numerical problem. The free-magnon contribution is

$$H_m = \sum_{\mathbf{q}} \hbar \omega_{\mathbf{q}} a_{\mathbf{q}}^\dagger a_{\mathbf{q}} \quad (3)$$

where $a_{\mathbf{q}}^\dagger$ ($a_{\mathbf{q}}$) are the creation (annihilation) operators for magnons on the ferromagnetic ground state with wave vector \mathbf{q} and energy $\hbar \omega_{\mathbf{q}}$, which we take to be

$$\hbar \omega(q) = D q^2 \quad (4)$$

with the magnon stiffness constant $D = 2 \text{ meV nm}^2$ and $q = |\mathbf{q}|$.

The electron-electron interaction is given by the standard expression

$$V_{e-e} = \frac{1}{2} \sum_{\mathbf{k} \mathbf{k}'} \sum_{\mathbf{q} \neq 0} v(q) \sum_{\sigma, \sigma'} c_{\mathbf{k}+\mathbf{q}, \sigma}^\dagger c_{\mathbf{k}'-\mathbf{q}, \sigma'}^\dagger c_{\mathbf{k}', \sigma'} c_{\mathbf{k}, \sigma} \quad (5)$$

where

$$v(q) = \frac{e^2}{\mathcal{V} \epsilon_0 q^2} \quad (6)$$

is the Coulomb potential with the normalization volume \mathcal{V} and vacuum dielectric constant ϵ_0 . For the treatment of Coulomb scattering and screening, we will follow Refs. [28, 29].

B. Magnons and Electron-Magnon Interaction

In the following we derive and subsequently solve a dynamical description of electron-magnon scattering. We separate the interacting ferromagnetic electron system in electronic single-particle states and their collective excitations, i.e., the magnons. Following Edwards [30], we introduce separate dynamical degrees of freedom for electrons and magnons by coupling band electrons to a Heisenberg model of localized spins, without assuming that the single-particle states correspond to quasi-free s -electrons and that the magnons arise as excitations of the more localized d -electrons, as in Refs. [27, 31]. The introduction of the localized spins is regarded as a formal way to capture the electronic properties related to collective dynamics [30] in order to avoid the considerable complications of a theory in which both single-particle and collective properties are determined from the interaction between d -electrons [32, 33]. Since we are interested in the far-from-equilibrium case, we do not use close-to-equilibrium response functions of the interacting electron system [34] or assume that the electronic system is in a quasi-equilibrium at all times during ultrafast demagnetization [20, 25, 27]. Once we have introduced the Heisenberg model we can go through a microscopic derivation using the coupling parameters of the model as in earlier treatments, which considered a spin system formed by well-localized electronic wave functions [35–37].

We next present a short version of the arguments of Refs. [35–37]. We write

$$H_{\text{spin}} = -J \sum_{\mathbf{R}} \mathbf{S}(\mathbf{R}) \cdot \mathbf{S}(\mathbf{R} + \boldsymbol{\delta}) \quad (7)$$

for the collective degrees of freedom, formed by a localized spin system with spins $\mathbf{S}(\mathbf{R})$ at lattice sites \mathbf{R} with

exchange constant J between neighboring spins. The interaction between these degrees of freedom and those associated with the itinerant electrons is taken to be

$$H_{\text{e-spin}} = -I\Omega \int \mathbf{S}(\mathbf{x}) \cdot \mathbf{s}(\mathbf{x}) d^3x, \quad (8)$$

where, following Ref. [37], we introduced a different exchange coupling constant I between the itinerant and localized spin densities. This is treated as a parameter in the present approach but can, in principle, be determined *ab initio*. We will assume a value of 0.9 eV, on the same order of magnitude as used by Beens et al. [25]. In Eq. (8) we have introduced the volume of a unit cell $\Omega \equiv \mathcal{V}/\mathcal{N}$ with the number of sites \mathcal{N} . For completeness we note the relation of the localized spins $\mathbf{S}(\mathbf{R})$ and the localized spin density $\mathbf{S}(\mathbf{x}) = \sum_{\mathbf{R}} \mathbf{S}(\mathbf{R})\delta(\mathbf{x} - \mathbf{R})$. In Ref. [37] the authors were interested in static renormalization effects, such as the shift of the band edge, which can be taken into account in the future, but for now we focus exclusively on the scattering dynamics between unrenormalized Bloch states. We employ the usual assumption that the spin density of the itinerant electrons

$$\mathbf{s}(\mathbf{x}) = \frac{1}{\mathcal{V}} \sum_{\mathbf{k}, \mathbf{k}'} \sum_{\sigma, \sigma'} \langle \mathbf{k}\sigma | \hat{\mathbf{s}} | \mathbf{k}'\sigma' \rangle e^{i(\mathbf{k}-\mathbf{k}') \cdot \mathbf{x}} c_{\mathbf{k}, \sigma}^\dagger c_{\mathbf{k}', \sigma'} \quad (9)$$

interacts with the localized spins at lattice sites \mathbf{R} . The Holstein-Primakoff transformation approximates the Fourier transformations of the localized spin operators

$$\mathbf{S}(\mathbf{R}) = \frac{1}{\sqrt{\mathcal{N}}} \sum_{\mathbf{q}} \mathbf{S}(\mathbf{q}) \exp(i\mathbf{q} \cdot \mathbf{R}) \quad (10)$$

by $S_+(\mathbf{q}) = S_x + iS_y = a_{\mathbf{q}}$, $S_-(\mathbf{q}) = S_x - iS_y = a_{-\mathbf{q}}^\dagger$ and $S_z(\mathbf{q}) = S - a_{\mathbf{q}}^\dagger a_{\mathbf{q}}$. The resulting Hamiltonian in second quantization is

$$V_{\text{e-m}} = -\frac{1}{\sqrt{\mathcal{N}}} \sum_{\mathbf{q}, \mathbf{k}} M_{\text{e-m}} \left(c_{\mathbf{k}+\mathbf{q}, \downarrow}^\dagger c_{\mathbf{k}, \uparrow} a_{\mathbf{q}} + c_{\mathbf{k}-\mathbf{q}, \uparrow}^\dagger c_{\mathbf{k}, \downarrow} a_{\mathbf{q}}^\dagger \right) \quad (11)$$

where $M_{\text{em}} = \frac{I}{2}$ is the matrix element for electron-magnon scattering.

The Hamiltonian (11) implies that electron-magnon scattering events are accompanied by a spin-flip in the

electronic system, as illustrated in Fig. 1. In a magnon-

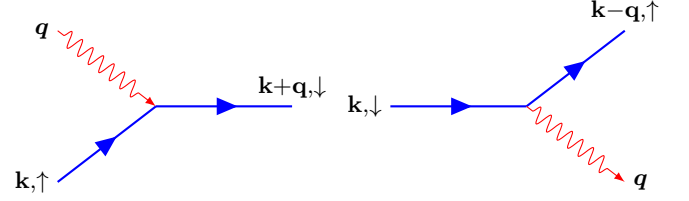


FIG. 1. Electronic spin-flip scattering processes due to magnon absorption (left) and magnon emission (right).

absorption vertex shown on the left of Fig. 1, an incoming spin-up electron with wave vector \mathbf{k} plus an incoming magnon with wave vector \mathbf{q} are connected to an outgoing spin-down electron with wave vector $\mathbf{k} + \mathbf{q}$. Conversely, in a magnon-emission vertex shown on the right of Fig. 1 an incoming spin-down electron with wave vector \mathbf{k} is connected to an outgoing spin-up electron with wave vector $\mathbf{k} - \mathbf{q}$ and an outgoing magnon with wave vector \mathbf{q} . Since the magnon contributes $-\hbar$ to the angular momentum balance, the total angular momentum is conserved at each vertex and thus in all transitions governed by this interaction.

Processes in which a magnon is emitted by a spin-up electron or in which a magnon is absorbed by a spin-down electron are not shown. These also need spin-orbit coupling, and are sometimes called anti-Stoner processes. They were found to be very small [21] and we neglect these completely [38].

The fundamental equations of motion in our approach are for the distribution functions of electrons $n_{\mathbf{k}, \sigma}$ and magnons $N_{\mathbf{q}}$. A derivation using the dynamical truncation of the hierarchy of equations of motion, which constitutes a general method for the derivation of coupled dynamical equations for the relevant correlation functions [39, 40], is presented in Appendix A. In this approach, incoherent transitions are described at the scattering level for the distributions of electrons and magnons. Denoting the ensemble average in the Heisenberg picture by $\langle \dots \rangle$, these are defined as $n_{\mathbf{k}, \sigma} = \langle c_{\mathbf{k}, \sigma}^\dagger c_{\mathbf{k}, \sigma} \rangle$, with $\sigma = \uparrow, \downarrow$, and $N_{\mathbf{q}} = \langle a_{\mathbf{q}}^\dagger a_{\mathbf{q}} \rangle$. The equations of motion then read

$$\left. \frac{\partial}{\partial t} n_{\mathbf{k}, \uparrow} \right|_{\text{e-m}} = \frac{2\pi}{\mathcal{N}\hbar} \sum_{\mathbf{q}} M_{\text{e-m}}^2 \delta(\epsilon_{\mathbf{k}}^\uparrow - \epsilon_{\mathbf{k}+\mathbf{q}}^\downarrow + \hbar\omega_{\mathbf{q}}) [n_{\mathbf{k}+\mathbf{q}, \downarrow} (1 - n_{\mathbf{k}, \uparrow}) (1 + N_{\mathbf{q}}) - N_{\mathbf{q}} n_{\mathbf{k}, \uparrow} (1 - n_{\mathbf{k}+\mathbf{q}, \downarrow})] \quad (12)$$

$$\left. \frac{\partial}{\partial t} n_{\mathbf{k}, \downarrow} \right|_{\text{e-m}} = \frac{2\pi}{\mathcal{N}\hbar} \sum_{\mathbf{q}} M_{\text{e-m}}^2 \delta(\epsilon_{\mathbf{k}}^\downarrow - \epsilon_{\mathbf{k}-\mathbf{q}}^\uparrow - \hbar\omega_{\mathbf{q}}) [N_{\mathbf{q}} n_{\mathbf{k}-\mathbf{q}, \uparrow} (1 - n_{\mathbf{k}, \downarrow}) - n_{\mathbf{k}, \downarrow} (1 + N_{\mathbf{q}}) (1 - n_{\mathbf{k}-\mathbf{q}, \uparrow})] \quad (13)$$

$$\left. \frac{\partial}{\partial t} N_{\mathbf{q}} \right|_{\text{e-m}} = \frac{2\pi}{\mathcal{N}\hbar} \sum_{\mathbf{k}} M_{\text{e-m}}^2 \delta(\epsilon_{\mathbf{k}+\mathbf{q}}^\downarrow - \epsilon_{\mathbf{k}}^\uparrow - \hbar\omega_{\mathbf{q}}) [n_{\mathbf{k}+\mathbf{q}, \downarrow} (1 - n_{\mathbf{k}, \uparrow}) (1 + N_{\mathbf{q}}) - N_{\mathbf{q}} n_{\mathbf{k}, \uparrow} (1 - n_{\mathbf{k}+\mathbf{q}, \downarrow})] \quad (14)$$

This system of dynamical equations contains in and out-scattering rates formally similar to those obtained from Fermi's Golden Rule [24, 27, 41], but the rates are calculated for the instantaneous values of the electron and magnon distributions, which may change considerably in time. Equations (12)–(14), in combination with the other processes detailed below, can therefore describe far-from-equilibrium situations. It is possible to consistently go beyond the scattering-level approximation by considering renormalization effects and electron-magnon coherences as well as including higher order terms and magnon-phonon coupling [27], but these extensions will be left to future studies.

C. Electron-Electron Interaction

For metallic systems or systems with itinerant electrons in general, the long-range Coulomb interaction, i.e.,

$$\begin{aligned} \left. \frac{d}{dt} n_{\mathbf{k},\sigma} \right|_{\text{e-e}} = & \frac{2\pi}{\hbar} \sum_{\sigma'\sigma'_1} \sum_{\mathbf{q}\mathbf{k}_1} \delta(\varepsilon_{\mathbf{k}}^{\sigma} + \varepsilon_{\mathbf{k}_1+\mathbf{q}}^{\sigma'_1} - \varepsilon_{\mathbf{k}+\mathbf{q}}^{\sigma'} - \varepsilon_{\mathbf{k}_1}^{\sigma'_1}) W_q(\sigma, \sigma_1, \sigma', \sigma'_1)^2 \\ & \times [n_{\mathbf{k}_1, \sigma'_1} n_{\mathbf{k}+\mathbf{q}, \sigma'} (1 - n_{\mathbf{k}_1+\mathbf{q}, \sigma_1}) (1 - n_{\mathbf{k}, \sigma}) - n_{\mathbf{k}_1+\mathbf{q}, \sigma_1} n_{\mathbf{k}, \sigma} (1 - n_{\mathbf{k}_1, \sigma'_1}) (1 - n_{\mathbf{k}+\mathbf{q}, \sigma'})]. \end{aligned} \quad (15)$$

Here we have approximated the dynamically screened Coulomb interaction by its static limit, that is, we employ the screened Coulomb matrix element

$$W_q(\sigma, \sigma_1, \sigma', \sigma'_1) = \frac{v(q)}{\tilde{\varepsilon}(q)} \times \begin{cases} 1, & \sigma = \sigma' \text{ and } \sigma_1 = \sigma'_1 \\ \alpha, & \sigma \neq \sigma' \text{ or } \sigma_1 \neq \sigma'_1 \\ \alpha^2, & \sigma \neq \sigma' \text{ and } \sigma_1 \neq \sigma'_1 \end{cases}. \quad (16)$$

where v_q is defined in Eq. (6). Importantly, this expression includes an effective EY spin-flip factor α [5, 14, 24, 42] to account for the overlap of non-pure spin states. If one does not consider the spin-orbit coupling in the basic Hamiltonian (1) in order to avoid dealing with the full spin density matrix, as included in Ref. [43], an approach with an α factor can give a good effective description of spin-flip processes in ferromagnets due to the interplay of electron-electron (or electron-phonon) interactions and spin-orbit coupling [13, 29]. We choose $\alpha = 0.1$, which, in principle, can be determined *ab initio*, but is also to be regarded as a parameter here. The dimensionless dielectric function is $\tilde{\varepsilon}(q)^{-1} = 1 + \kappa^2/q^2$ where κ is the screening parameter, which we estimated according to the Thomas-Fermi screening to be $\kappa = \sqrt{e^2/\varepsilon_0} \partial n_e / \partial \mu = 5.12 \text{ nm}^{-1}$, where n_e is the electron density. The contribution $\delta(\varepsilon_{\mathbf{k}}^{\sigma} + \varepsilon_{\mathbf{k}_1+\mathbf{q}}^{\sigma'_1} - \varepsilon_{\mathbf{k}+\mathbf{q}}^{\sigma'} - \varepsilon_{\mathbf{k}_1}^{\sigma'_1})$ guarantees the energy conservation for this two-electron scattering process [28]. Note that these scattering processes conserve the total number of electrons, total electron energy and total electron momentum, since we

electron-electron scattering is important on ultrashort timescales such as those of the demagnetization process, and we therefore need to include their effect. [28, 32]. The interaction vertex is shown in the sketch in Fig. 2.

At the level corresponding to our treatment of electron-magnon scattering, one finds that the spin dependent equation of motion due to electron-electron interaction for the distribution functions $n_{\mathbf{k}\sigma}$ at wave vector \mathbf{k} in band σ can be expressed in the form [14]

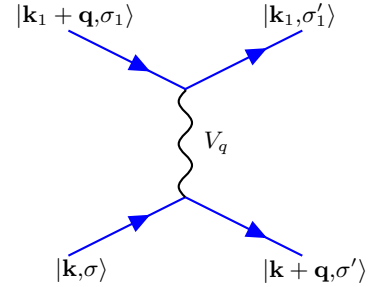


FIG. 2. Scattering process between electrons with spins σ and σ_1 in states $|\mathbf{k}, \sigma\rangle$, $|\mathbf{k}_1 + \mathbf{q}, \sigma_1\rangle$ leading to final states $|\mathbf{k} + \mathbf{q}, \sigma'\rangle$, $|\mathbf{k}_1, \sigma'_1\rangle$ with spins σ' and σ'_1 due to the Coulomb interaction V_q .

exclude umklapp scattering. The total electron spin is not conserved, as we use Bloch states, which are nonpure spin states. In this case, the lattice acts as a spin sink when the electronic spin state is changed in an incoherent transition from an initial to a final state.

D. Electron-Phonon and Magnon-Phonon Interactions

We describe electronic energy relaxation processes that occur due to the electron-phonon interaction using a

relaxation-time approximation

$$\left. \frac{\partial n_{\mathbf{k},\sigma}}{\partial t} \right|_{\text{e-p}} = -\frac{n_{\mathbf{k},\sigma}(t) - n_{\mathbf{k},\sigma}^{(\text{eq})}}{\tau_{\text{e-p}}}, \quad (17)$$

where

$$n_{\mathbf{k},\sigma}^{(\text{eq})} = f_{\text{FD}}(\epsilon_{\mathbf{k},\sigma} - \mu(n_{\sigma}, T_{\text{L}})) \quad (18)$$

are Fermi-Dirac distributions that are computed from the dynamical electron distributions $n_{\mathbf{k},\sigma}(t)$. The Fermi-Dirac distributions replicate the instantaneous electron density n_{σ} in each band σ , but are determined with the equilibrium temperature of the lattice, which is kept fixed throughout the dynamics at the lattice temperature $T_{\text{L}} = 300$ K. This approximation, which introduces the relaxation time $\tau_{\text{e-p}}$ as its characteristic time scale, is made here because electron-phonon scattering occurs on a longer timescale than both electron-electron and electron-magnon scattering so that a microscopic treatment is less important. Note that the contribution (17) by itself does not change the total spin of the electronic system, i.e., it does not include spin-flips due to electron-phonon scattering in connection with spin-orbit coupling.

In the numerical results presented below it turns out that the coupling of the magnons to phonons also plays a significant role. In order to describe the effect of such a coupling we also use a relaxation-time approximation, which here takes the form

$$\left. \frac{\partial N_{\mathbf{q}}}{\partial t} \right|_{\text{m-p}} = -\frac{N_{\mathbf{q}}(t) - N_{\mathbf{q}}^{(\text{eq})}}{\tau_{\text{m-p}}}. \quad (19)$$

We again make a bath assumption for the phonons, i.e., we use an equilibrium Bose distribution $N_{\mathbf{q}}^{(\text{eq})}$ at the lattice temperature. The characteristic time scale is set by the magnon-phonon relaxation time $\tau_{\text{m-p}}$. Equation (19) describes the thermalization of the magnon system via processes that change the total number of magnons, i.e., both total magnon energy and total magnon angular momentum are changed.

The equations for the dynamics of electrons and magnons, which form the basis of the results presented in Sec. III, are Eqs. (12)–(14), (15), (17) and (19). As the scattering processes described by Eqs. (12)–(14) and (15) conserve the total number of electrons, it is important to also ensure this conservation for the numerical solution because differences in the distributions, such as the polarization P defined in (23) play an important role. In these quantities, small deviations from a complete number-density conservation may potentially yield large numerical errors.

E. Electronic Band Structure

The description of scattering processes has been fairly general so far and needs to be augmented by specifying the electronic Bloch states connected in these transitions.

As a simple model of electronic states in a ferromagnet we consider a band structure with two bands that are separated by a Stoner splitting. For definiteness, we refer to the majority electrons as spin-up electrons and the minority carriers as spin-down, as shown in Fig. 3. We choose a modified tight binding (TB) band structure of the form

$$\begin{aligned} \epsilon_{\mathbf{k},\uparrow} &= \epsilon_0 - 2\gamma \cos(ka_0) \\ \epsilon_{\mathbf{k},\downarrow} &= \epsilon_{\mathbf{k},\uparrow} + \Delta \end{aligned} \quad (20)$$

where γ is the hopping energy that controls the band width, which is in 1D equal to 4γ , and Δ is the Stoner spin splitting energy. While this result applies to a one-dimensional lattice, we use it here with the modulus $k = |\mathbf{k}|$ of a three-dimensional vector. Such a “spherical approximation” makes it easier to numerically evaluate the time dependent scattering integrals with momentum dependent scattering kernels in the dynamics. This simplification can, in principle, be removed, but only at a very considerable computational cost because of the integrations over anisotropic distributions on a three-dimensional k grid.

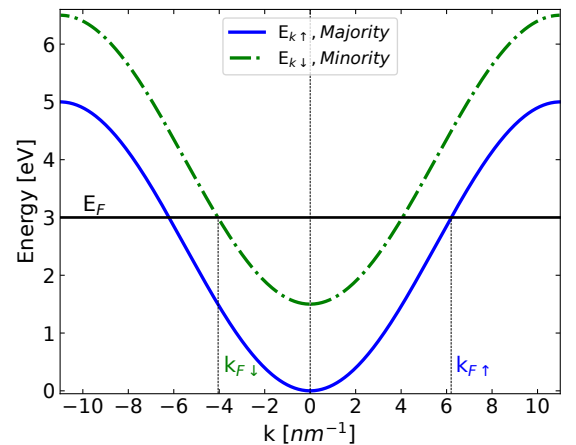


FIG. 3. Band dispersion for spin-up (majority) and spin-down (minority) electrons, with a lattice constant a_0 of 2.86 \AA and a band width 4γ of 5 eV [30]. The electron density is chosen such that the self-consistently calculated ground state results in a spin splitting Δ of 1.5 eV [44].

The Stoner splitting is given by

$$\Delta = U_{\text{eff}}(n_{\uparrow} - n_{\downarrow}) \quad (21)$$

where n_{σ} is the number of electrons per unit cell in the majority/minority channel, respectively,

$$n_{\sigma} := \frac{1}{\mathcal{N}} \sum_{\mathbf{k}} n_{\mathbf{k},\sigma}, \quad (22)$$

and U_{eff} an effective Hubbard electrostatic repulsion energy [36]. The Stoner splitting Δ is self-consistently calculated for the thermal-equilibrium case. We will also discuss the influence of a time-dependent splitting $\Delta(t)$ which is calculated from the instantaneous values of $n_{\sigma} = n_{\sigma}(t)$ [15].

III. RESULTS AND DISCUSSION

A. Spin Polarization, Magnetization and Their Connection

Electrons and magnons can, in principle, contribute to the total magnetization of the system, as they both carry angular momentum. The question how to correctly account for this influence on the different effects that are used to experimentally characterize the out-of-equilibrium magnetization is complicated. We follow here Refs. [25, 26] and combine the spin polarization with the magnon angular momentum to obtain a measure of the total transient magnetization of the system. Switching to dimensionless quantities, we will call the magnetization contribution of the electronic system *spin polarization* P , which is defined as

$$P = \frac{n_{\uparrow}(t) - n_{\downarrow}(t)}{2} \quad (23)$$

where $n_{\uparrow/\downarrow}$ are the number of majority and minority electrons per unit cell defined in Eq. (22). The contribution of the magnons is the *magnon magnetization*

$$M = -\delta N(t) \equiv -[N(t) - N_0], \quad (24)$$

which is given by the change in the number of magnons

$$N(t) = \sum_{\mathbf{q}} N_{\mathbf{q}} \quad (25)$$

with respect to that in equilibrium N_0 . The total magnetization m , is then determined as

$$m = M + P. \quad (26)$$

B. Electronic Distribution Function Dynamics

In this and the following subsections we numerical results for the coupled electron and magnon dynamics due to the contribution of spin-flip electron-electron and electron-magnon (e-e-m) scattering processes combined with electron-phonon and magnon-phonon relaxation processes discussed in Sec. II. We first focus on the microscopic energy resolved distributions of electrons and magnons, as they result from the numerical solution of Eqs. (12)–(14), (15), (17) and (19). From these, ensemble averaged quantities are calculated, in particular the magnetization, for which the physics is discussed starting in Sec. IIID.

In an experiment, demagnetization is triggered by excitation with an ultrashort pulse. In order to capture some characteristics of an optical-pulse excitation, we will consider here an instantaneous excitation in the electronic system, which replaces the equilibrium distribution functions in each spin channel with hot Fermi-Dirac distributions at an electronic temperature of 2000 K of the same

density. This process instantaneously creates “hot” electrons without changing the equilibrium spin polarization, i.e., the band structure, specifically the splitting Δ , is not changed by the excitation. The resulting “hot” distribution functions are characterized by a change of the chemical potential of roughly 27 meV and a spin accumulation of $\zeta = \mu_{\uparrow} - \mu_{\downarrow} = 0.6$ meV, where the chemical potentials refer to the “hot” Fermi-Dirac distributions with the same spin polarization as the equilibrium system. Below, we will also use fits by Fermi-Dirac and Bose distributions, respectively, in order to describe the energy and spin polarization by time dependent intensive quantities $T(t)$ and $\mu_s(t)$. However, the underlying distributions are computed dynamically and never assumed to be exact Fermi-Dirac or Bose distributions.

We employ relaxation-time approximations 17, (19) for the interaction of electrons and magnons with phonons and choose values of $\tau_{e-p} = 1$ ps [45–47] and $\tau_{m-p} = 10$ ps [48], respectively. The magnon-phonon process is included here to ensure that the system eventually reaches a complete equilibrium. The numerical value of the magnon-phonon relaxation time is such that the demagnetization process at early times remains essentially unaffected. The importance of the relaxation contributions will be discussed in more detail below.

Since we aim at describing a metallic system at high densities, only electrons around and above the Fermi energy play an important role in the dynamics. Their contribution to the k-resolved carrier distribution is

$$\delta n_{\mathbf{k},\sigma} \equiv n_{\mathbf{k},\sigma} - f_{F-D}(\epsilon_{\mathbf{k},\sigma} - \mu) \quad (27)$$

where we subtract the Fermi-Dirac distribution function for the electrons at equilibrium before excitation, including the equilibrium chemical potential μ . Figure 4 shows the changes in majority $\delta n_{\mathbf{k}\uparrow}$ (a) and minority carriers $\delta n_{\mathbf{k}\downarrow}$ (b) at different times. The instantaneous excitation at $t = 0$ leads to a dipolar shape (black lines), which indicates a redistribution of electrons from below to above the Fermi edge.

The dashed red curve in Fig. 4 shows that minority electrons, i.e., carriers in states with energies above E_F are dominantly scattered into majority states ($e_{\downarrow} \rightarrow e_{\uparrow}$). If we refer to carriers below the Fermi level, $E < E_F$, as holes (h), then majority holes are scattered to minority states ($h_{\uparrow} \rightarrow h_{\downarrow}$) at very early times during the scattering dynamics. The snapshot at 33 fs has been selected as it shows the maximum of this effect, i.e., when the electronic spin polarization reaches a *maximum*, highlighting the deviation from equilibrium in the electronic dynamics.

The increase in spin polarization is an important characteristic of electron-magnon scattering, as discussed in Sec. IIID in more detail. At later times, cf. the blue dash dotted and the green dotted lines in Fig. 4, the δn s decay as the carrier distributions approach their equilibrium values on the time scale set by the electron-phonon and electron-magnon relaxation times.

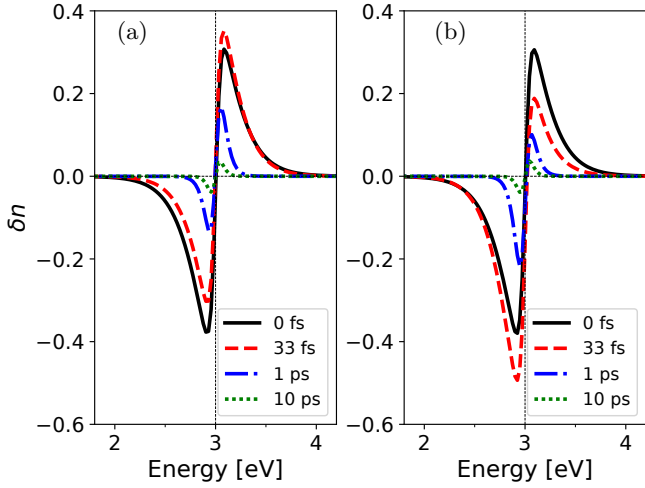


FIG. 4. Distribution functions of majority (a) and minority (b) electrons for different times during scattering dynamics (e-e + e-m) with electron-phonon relaxation and magnon-phonon relaxation after instantaneous excitation at $t = 0$. The red curve shows that minority electrons are initially scattered into empty majority states. The distribution functions $\delta n_{\mathbf{k},\sigma}$ are plotted here vs. energy.

C. Coupled Dynamics of Electrons and Magnons

This subsection focuses on the non-equilibrium magnon distributions as obtained from evaluating Eq. (14), which sensitively depend on the available scattering phase space for electronic transitions between minority and majority states. Such transitions $|\mathbf{k}, \uparrow\rangle \rightarrow |\mathbf{k} + \delta\mathbf{k}, \downarrow\rangle$ due to electron-magnon scattering with momentum transfer $\delta\mathbf{k}$ lead to an electronic energy change

$$\delta\epsilon = \epsilon_{\mathbf{k}+\delta\mathbf{k}} - \epsilon_{\mathbf{k}} + \Delta. \quad (28)$$

in the band structure of Fig. 3. In Fig. 5(a), the shaded area is the so-called Stoner continuum, i.e., those values of the energy change (28) achievable for transitions connecting occupied majority states $|\mathbf{k}| \leq k_{F,\uparrow}$ with unoccupied minority states $|\mathbf{k} + \delta\mathbf{k}| \leq k_{F,\downarrow}$. Figure 5(a) also shows the magnon dispersion (4) and its crossing points with the Stoner continuum. Electronic spin-flip transitions can only couple to magnons with wave vectors q between points δk_{\min} and δk_{\max} .

Figure 5(b) plots the dynamical change in the magnon distribution $\delta N_q = N_q(t) - N_q^{(\text{eq})}(T_{\text{lattice}})$. We assume that magnons are not directly excited, so that the black line in Fig. 5(b) at $t = 0$ is flat, $\delta N_q(t = 0) = 0$. After the instantaneous excitation process, only magnons in the wave-vector range between δk_{\min} and δk_{\max} are absorbed and emitted. This is the range where the magnon dispersion overlaps with the Stoner continuum. In more detail, during the early stages of the coupled dynamics, shown here for 50 fs and 0.5 ps, magnons at long wavelengths, i.e., q near q_{\min} are predominantly absorbed, whereas those at shorter wavelengths, i.e. q between

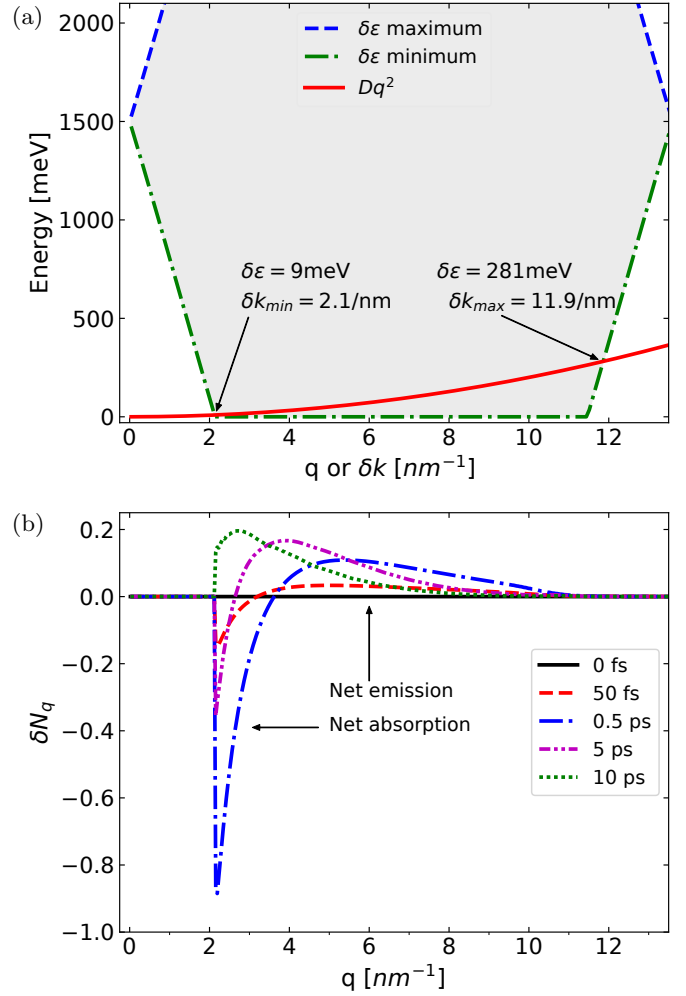


FIG. 5. (a) Stoner continuum of electronic spin-flip transitions and magnon dispersion. The overlap occurs between $q_{\min} = 2.1/\text{nm}$ and $q_{\max} = 11.9/\text{nm}$. (b) Magnon distribution functions at different times due to scattering with electrons in a band structure with constant exchange splitting. The magnon distributions are changed only in the q region that overlaps with the Stoner continuum.

$q \simeq 3 \text{ nm}^{-1}$ and q_{\max} , are predominantly emitted. The absorption for small q is much weaker than the emission for large q , because the total change in magnon density is calculated according to Eq. (25) as

$$N(t) = \frac{\Omega}{2\pi^2} \int q^2 N_q dq \quad (29)$$

including the weight factor of q^2 . At longer times, shown here for 5 ps and 10 ps, the absorption range of δN_q slowly shrinks until there is no trace left while the peak resulting from effective magnon emission shifts towards q_{\min} . Even for 10 ps the magnon distributions still have not returned to equilibrium, and the same is true for the electronic distributions in Fig. 4.

Figure 6 plots the effective temperatures of electrons and magnons after the instantaneous excitation. We

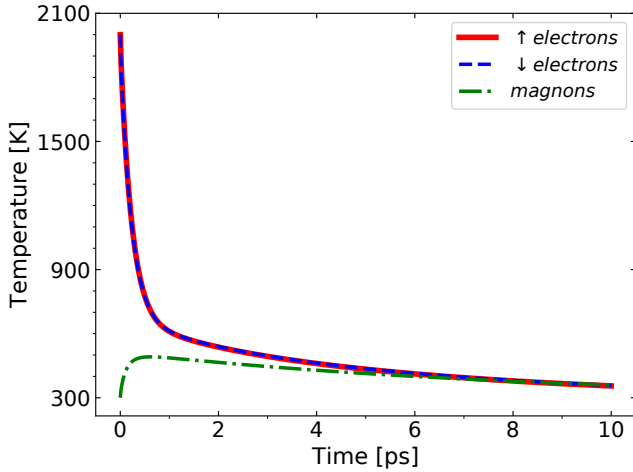


FIG. 6. Temperature of electrons and magnons during scattering dynamics. Only electrons are excited at 2000 K while the magnons are kept at the lattice temperature 300 K.

stress that these effective temperatures are those of equilibrium distributions with the same particle number and energy densities as those of the dynamical distributions, and show the energy exchange between electrons, magnons, and the lattice. They are determined by fits to the calculated dynamical distributions. At all times, the effective temperatures for spin-up and spin-down electrons are almost equal, due to the excitation condition and the fast electron-electron scattering. At times shorter than a picosecond, most of the energy is exchanged between electrons and magnons due to their interaction as the instantaneous excitation opens up scattering phase space. The magnons take about 0.5 ps until their maximum effective temperature of roughly 500 K is reached. At this point, the blue dash dotted line in Fig. 5(b) shows that the deviation of the magnon distribution function from its equilibrium is most pronounced. After approximately 7 ps, the energy transfer from electrons to magnons has slowed down and a quasi-equilibrium situation is reached, in which the common electron and magnon temperature still differs from that of the lattice. Complete thermal equilibrium, at which all temperatures are equal to 300 K, is only approached on the time scale of the magnon-phonon relaxation.

D. Spin Polarization and Magnetization Dynamics

After the characterization of the electron and magnon dynamics at the level of microscopic momentum resolved distributions, we now turn to the macroscopic quantities, in particular the magnetization dynamics. In Fig. 7 we investigate the different contributions to the magnetization as defined in Eqs. (23)–(26). We consider in this section the cases of a fixed splitting Δ and a dynamically calculated $\Delta(t)$ [15], which changes the electronic quasi-

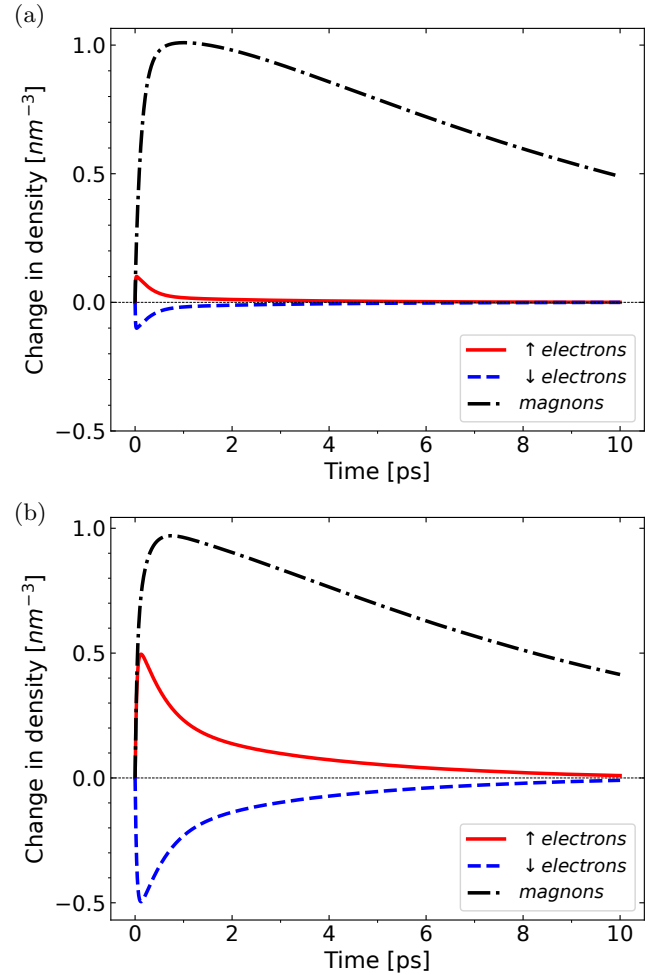


FIG. 7. Density change for electrons with spin up (solid line), electrons with spin down (dashed blue line) and magnons during e-e-m- r_{ep} - T_{mp} with (a) constant spin splitting, and (b) dynamical spin splitting.

particle states. At the end, we compare both scenarios, but the main conclusion can already be drawn by considering the case with constant Δ , which we discuss in detail first.

Figure 7 plots the change in the electronic $\delta n_{\uparrow/\downarrow}$ and magnon densities δN . The changes of the electronic densities have the same magnitude but opposite sign, so that the electronic spin-polarization is just $P = \delta n_{\uparrow}$, cf. Eq. (23), whereas the magnon magnetization M is the change in magnon density plotted in Fig. 7 with opposite sign. At very early times, the electronic spin polarization *increases* as magnons are created, which is the net effect when integrating the change in the magnon distribution δN_q as shown in Fig. 5(b) over all wave vectors q , cf. Eqs. (24)–(25). In the case of a constant gap as shown in Fig. 7(a) the change in magnon density is almost 10 times larger than the density of the electronic spins flipped, or, equivalently, the decrease in M is 10 times larger than the increase in P . The effect of the scattering processes

is, therefore, to produce a change in the magnon magnetization that is an order of magnitude larger than the change in the spin polarization.

This imbalance is an important result, because electron-magnon scattering alone leads to changes in magnon density that *exactly equal* the electronic spin-polarization change, because the angular-momentum conservation is implicitly included in Eqs. (11)–(14). The large discrepancy between M and P in Fig. 7(b) can be explained by the *interplay* of electron-magnon with EY-type electron-electron scattering as follows. On the timescale on which most of the energy is transferred from the electronic to the magnon system, as shown in Fig. 6, electron-magnon scattering creates magnons in a process that transfers angular momentum into the electronic system, as sketched in Fig. 1. The electron-magnon scattering processes thereby increase the spin polarization or, equivalently, lead to a non-equilibrium spin accumulation $\zeta = \mu_{\uparrow}(t) - \mu_{\downarrow}(t)$. We reiterate that the chemical potentials $\mu_{\sigma}(t) = \mu(n_{\sigma}(t), T_{\sigma}(t))$ and effective temperatures $T_{\sigma}(t)$ refer to Fermi-Dirac distributions in each band that have the same density and energy density as the non-equilibrium distributions $n_{\mathbf{k},\sigma}(t)$. The non-equilibrium spin accumulation in the electronic systems is the driving force for EY-type electron-electron scattering [49], which effectively relaxes the spin polarization and, in turn, frees up scattering phase space in the electronic system for spin-flip transitions that create more magnons. The two processes can support each other until the maximum magnon density is reached. At that time, the electronic system has cooled down so much that the electron-magnon scattering has only little scattering phase-space left.

It is interesting to compare the combination of scattering processes with the electron-electron scattering of Elliott-Yafet-type acting alone, i.e., without magnons [14, 15]. In this case we would find a *decrease* of the spin-polarization compared to its equilibrium value, because EY-like scattering relaxes the spin accumulation, which is created by the instantaneous heating process with a sign opposite to that driven by electron-magnon scattering. The absolute value of the change in spin polarization would be considerably smaller (not shown) than what is shown in Fig. 7(a) for the band structure and excitation conditions of the present paper.

We now turn to the results of the calculation including the dynamical splitting in Fig. 7(b). Qualitatively the same observations hold true here, but the maximum transient electronic spin polarization is about 5 times larger than that occurring for the constant splitting in Fig. 7(a) and appears later at approximately 130 fs. The dynamical gap, i.e., an instantaneous change of the mean-field (21), amplifies the change in electronic spin polarization compared with the case of a static gap, as the change in splitting increases the available phase space for whatever process drives the spin-changing transitions in the electronic system. In Ref. [15], where the case of a pure EY-like scattering processes with electrons and phonons

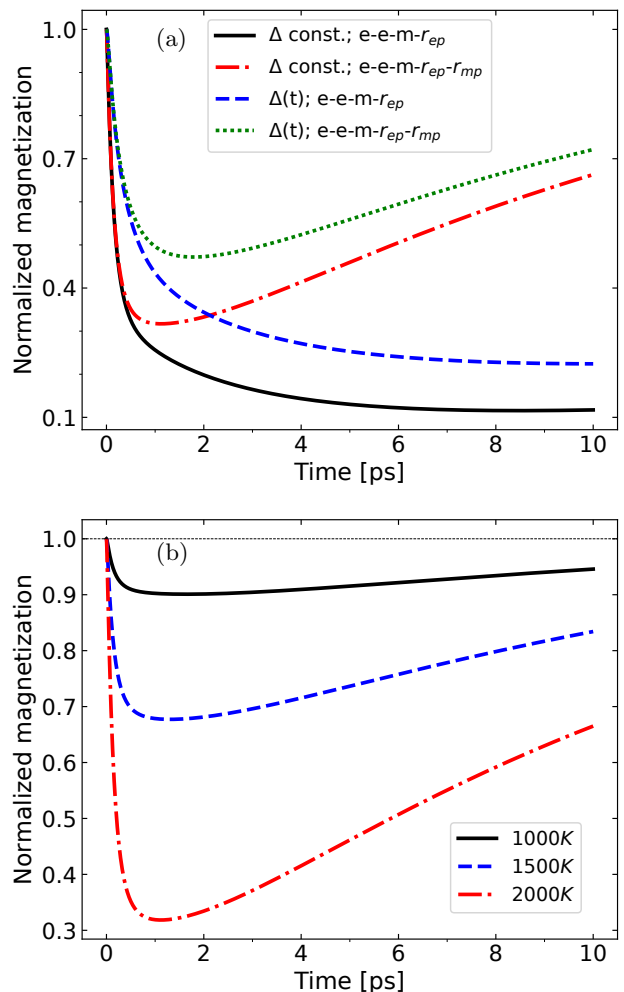


FIG. 8. Dynamics of the magnetization $m(t)$ after instantaneous heating due to e-e-m scattering together with electron-phonon relaxation (r_{ep}). (a) Results computed with constant/dynamic splitting Δ and additional magnon-phonon relaxation (r_{mp}), see legend. (b) Magnetization dynamics with e-e-m- r_{ep} - r_{mp} contributions and constant splitting Δ for different excitation temperatures.

was considered, this interplay of the scattering processes with the dynamical gap leads to a stronger decrease of the spin polarization after an instantaneous heating.

Figure 8 shows the dynamics of the magnetization $m(t)$ normalized to the electronic polarization in equilibrium. As before, we include electron-phonon and magnon-phonon interactions as relaxation processes, but ignore the magnon-phonon relaxation in some of the results to highlight its impact. While Fig. 8(a) focuses on the impact of magnon-phonon relaxation and on the difference between a constant and dynamic Stoner splitting, Fig. 8(b) illustrates the influence of the excitation strength by varying the temperature of the initial hot Fermi-Dirac distribution.

We first consider those results in Fig. 8(a) that include

only electron-phonon relaxation processes. In this case, the magnetization steadily decreases, with a stronger demagnetization in the constant-gap case. The total magnetization $m = M + P$ is quenched less for the case of the dynamical gap. The difference is almost exclusively due to the contributions of the electronic spin polarization P , cf. Fig. 7. For longer times, the magnetization approaches a constant value, which is a result of “frozen out” magnons. These are non-equilibrium magnons created by the electron-magnon scattering at earlier times at q values that are not accessible any more due to a lack of electronic scattering partners in the equilibrated electron distributions. It seems that, in order for the magnons to relax, a direct coupling of phonons to magnons is necessary, which led us to include a magnon-phonon relaxation term at the outset.

The results in Fig. 8(a) that include such a magnon-phonon relaxation contribution resemble the typical shape of demagnetization dynamics usually observed experimentally where the ultrafast demagnetization is followed by a remagnetization on a 10 ps time scale. It is evident that a dynamical gap reduces the minimal magnetization due to a more pronounced increase in spin polarization.

In Fig. 8(b) we study the influence of the energy deposited in the electronic system on the demagnetization process. We find that a smaller quenching of about 30% and 10% results for 1500 K and 1000 K, respectively, while maintaining the same overall shape and time scales of the demagnetization and remagnetization dynamics. The deposited energies per unit cell due to the excitation are 8.8 meV, 20.9 meV, 38.1 meV for 1000 K, 1500 K, 2000 K. Fig. 8(b) are also on the same order of magnitude as in typical experiments [6, 50]

These results for the demagnetization dynamics suggest that non-equilibrium magnons play an important role in the demagnetization process and that different magnon-interaction processes are involved in the demagnetization and remagnetization dynamics. The model assumptions, such as the simplified band structure and excitation processes, can be improved in the future, so that eventually it should be possible to obtain the achievable demagnetization for a realistic material excitation and compare these with experiments. This is likely the most important test a demagnetization mechanism has to pass, as there are many processes that can to some extent influence the magnetization. The question is, in our view: can any given process explain the demagnetization signal for a realistic experimental fluence, i.e., deposited energy per unit cell.

IV. CONCLUSION

We investigated the dynamics of electrons in ferromagnets on ultrashort timescales due to electron-magnon and spin-flip electron-electron scattering in the framework of a microscopic model. In this model the dom-

inant interactions between electrons and magnons that change the electronic spin involve high- q magnons for which the dispersion crosses the (q, ω) region of Stoner excitations. After an instantaneous excitation process, which opens up electronic scattering phase space, non-equilibrium magnon distributions are created. While electron-magnon scattering by itself leads to an *increase* of the electronic spin polarization that is equal in magnitude but opposite to the decrease of angular momentum due to the emission of magnons. This balance between spin polarization and magnon magnetization is broken if one includes an Elliott-Yafet like spin-flip scattering which occurs due to the interplay of spin-orbit coupling and electron-electron scattering. The Elliott-Yafet spin-flip scattering provides a spin relaxation mechanism for the electronic spin polarization that facilitates a larger demagnetization due to efficient magnon emission. This is because the scattering processes creating the magnons also increase the spin polarization, which then drives the Elliott-Yafet spin-relaxation mechanism. From our model calculations one can draw the conclusion that ultrafast demagnetization involves mainly the emission of magnons, with only a comparatively small contribution of the spin polarization created in the electronic system. We only obtain a remagnetization behavior in accordance with experimental results if we include a phenomenological magnon-phonon coupling. Without this coupling the remagnetization process due to the combination of electron-magnon and electron-phonon scattering results in a steady state with non-equilibrium magnon distributions that cannot change due to scattering with the equilibrated electron system. This result points to the importance of magnon-phonon interactions, which we will study in a microscopic fashion in the framework of this model in the near future.

ACKNOWLEDGMENTS

This work was funded by the Deutsche Forschungsgemeinschaft (DFG, German Research Foundation) through grant No. TRR 173-268565370 (projects B03, A08) and Deutscher Akademischer Austauschdienst (DAAD, German Academic Exchange Service).

Appendix A: Derivation of Electron-Magnon Scattering Contributions

In this Appendix, we derive the scattering contributions to the equations of motion for the distribution function of electrons and magnons due to electron-magnon interaction using a truncation of the hierarchy of the equations of motion [39, 40, 51]. The equation of motion for electron distributions such as $n_{\mathbf{k},\downarrow} = \langle c_{\mathbf{k},\downarrow}^\dagger c_{\mathbf{k},\downarrow} \rangle$ is given

by

$$i\hbar \frac{\partial}{\partial t} n_{\mathbf{k},\downarrow} \Big|_{\text{e-m}} = -\frac{M_{\text{e-m}}}{\sqrt{\mathcal{N}}} \sum_{\mathbf{q}} (\langle a_{\mathbf{q}} c_{\mathbf{k},\downarrow}^{\dagger} c_{\mathbf{k}-\mathbf{q},\uparrow} \rangle - \text{c. c.}) \quad (\text{A1})$$

where electron-magnon correlations of the form $\langle a c_{\downarrow}^{\dagger} c_{\uparrow} \rangle$ appear.

Similarly, the distribution function of magnons is given by

$$i\hbar \frac{\partial}{\partial t} N_{\mathbf{q}} \Big|_{\text{e-m}} = \frac{M_{\text{e-m}}}{\sqrt{\mathcal{N}}} \sum_{\mathbf{k}} [\langle a_{\mathbf{q}} c_{\mathbf{k},\downarrow}^{\dagger} c_{\mathbf{k}-\mathbf{q},\uparrow} \rangle - \text{c. c.}] \quad (\text{A2})$$

The electron-magnon correlation function obeys

$$i\hbar \partial_t \langle a_{\mathbf{q}} c_{\mathbf{k},\downarrow}^{\dagger} c_{\mathbf{k}-\mathbf{q},\uparrow} \rangle = -\frac{M_{\text{e-m}}}{\sqrt{\mathcal{N}}} \left\{ \sum_{\mathbf{k}'} \langle c_{\mathbf{k}'-\mathbf{q},\uparrow}^{\dagger} c_{\mathbf{k}',\downarrow} c_{\mathbf{k},\downarrow}^{\dagger} c_{\mathbf{k}-\mathbf{q},\uparrow} \rangle + \sum_{\mathbf{q}'} [\langle a_{\mathbf{q}} a_{\mathbf{q}'}^{\dagger} c_{\mathbf{k},\downarrow}^{\dagger} c_{\mathbf{k}-\mathbf{q}+\mathbf{q}',\downarrow} \rangle - \langle a_{\mathbf{q}} a_{\mathbf{q}'}^{\dagger} c_{\mathbf{k}-\mathbf{q}',\uparrow}^{\dagger} c_{\mathbf{k}-\mathbf{q},\uparrow} \rangle] \right\} \quad (\text{A3})$$

At the scattering level, the equation of motion for the electron-magnon correlation is closed by replacing higher-order correlations by products of lower-order correlations, such as

$$\langle c_{\mathbf{k}'-\mathbf{q},\uparrow}^{\dagger} c_{\mathbf{k}',\downarrow} c_{\mathbf{k},\downarrow}^{\dagger} c_{\mathbf{k}-\mathbf{q},\uparrow} \rangle = \delta_{\mathbf{k},\mathbf{k}'} \langle c_{\mathbf{k}'-\mathbf{q},\uparrow}^{\dagger} c_{\mathbf{k}-\mathbf{q},\uparrow} \rangle - \langle c_{\mathbf{k}'-\mathbf{q},\uparrow}^{\dagger} c_{\mathbf{k},\downarrow}^{\dagger} c_{\mathbf{k}',\downarrow} c_{\mathbf{k}-\mathbf{q},\uparrow} \rangle \simeq \delta_{\mathbf{k},\mathbf{k}'} n_{\mathbf{k}-\mathbf{q},\uparrow} (1 - n_{\mathbf{k},\downarrow}) \quad (\text{A4})$$

and, similarly, $\langle a_{\mathbf{q}} a_{\mathbf{q}'}^{\dagger} c_{\mathbf{k},\downarrow}^{\dagger} c_{\mathbf{k}-\mathbf{q}+\mathbf{q}',\downarrow} \rangle \simeq \delta_{\mathbf{q},\mathbf{q}'} (1 + N_{\mathbf{q}}) n_{\mathbf{k},\downarrow}$. With these replacements, the electron-magnon correlation dynamics is given by

$$i\hbar \frac{\partial}{\partial t} \langle a_{\mathbf{q}} c_{\mathbf{k},\downarrow}^{\dagger} c_{\mathbf{k}-\mathbf{q},\uparrow} \rangle = -(\epsilon_{\mathbf{k}}^{\downarrow} - \epsilon_{\mathbf{k}-\mathbf{q}}^{\uparrow} - \hbar\omega_{\mathbf{q}} + i\hbar\gamma) \langle a_{\mathbf{q}} c_{\mathbf{k},\downarrow}^{\dagger} c_{\mathbf{k}-\mathbf{q},\uparrow} \rangle + \frac{1}{\sqrt{\mathcal{N}}} M_{\text{e-m}} [N_{\mathbf{q}} n_{\mathbf{k}-\mathbf{q},\uparrow} (1 - n_{\mathbf{k},\downarrow}) - n_{\mathbf{k},\downarrow} (1 + N_{\mathbf{q}}) (1 - n_{\mathbf{k}-\mathbf{q},\uparrow})] \quad (\text{A5})$$

where we have included a decay constant γ that approximates the influence of higher-order contributions. This equation has the general form

$$i\hbar \frac{\partial}{\partial t} X = -(\Delta E + i\hbar\gamma) X + i\hbar\Gamma, \quad (\text{A6})$$

which is very similar to the corresponding quantity for phonon-assisted electronic distributions. The formal so-

lution of Eq. (A6) is given by [11, 51]

$$X(t) = \frac{1}{i\hbar} \int_{-\infty}^t d\tau \Gamma(\tau) e^{i[\Delta E/\hbar + i\gamma](t-\tau)}, \quad (\text{A7})$$

Using the Markov approximation, which assumes that $\Gamma(\tau)$ varies slowly compared to the rotation frequency $\Delta E/\hbar$ and can be approximated as $\Gamma(t)$, this equation can be analytically solved, yielding

$$X(t) = \frac{\Gamma(t)}{\Delta E + i\hbar\gamma}. \quad (\text{A8})$$

If $\gamma \rightarrow 0$, we have $X(t) = \Gamma(t)[\text{p.v.} \frac{1}{\Delta E} - i\pi\delta(\Delta E)]$ and one obtains

$$\begin{aligned} \langle a_{\mathbf{q}} c_{\mathbf{k},\downarrow}^{\dagger} c_{\mathbf{k}-\mathbf{q},\uparrow} \rangle &= \frac{M_{\text{e-m}}}{\sqrt{\mathcal{N}}} \frac{[N_{\mathbf{q}} n_{\mathbf{k}-\mathbf{q},\uparrow} (1 - n_{\mathbf{k},\downarrow}) - n_{\mathbf{k},\downarrow} (1 + N_{\mathbf{q}}) (1 - n_{\mathbf{k}-\mathbf{q},\uparrow})]}{(\epsilon_{\mathbf{k}}^{\downarrow} - \epsilon_{\mathbf{k}-\mathbf{q}}^{\uparrow} - \hbar\omega_{\mathbf{q}}) + i\gamma} \\ &= -\frac{i\pi}{\sqrt{\mathcal{N}}} \delta(\epsilon_{\mathbf{k}}^{\downarrow} - \epsilon_{\mathbf{k}-\mathbf{q}}^{\uparrow} - \hbar\omega_{\mathbf{q}}) M_{\text{e-m}} [N_{\mathbf{q}} n_{\mathbf{k}-\mathbf{q},\uparrow} (1 - n_{\mathbf{k},\downarrow}) - n_{\mathbf{k},\downarrow} (1 + N_{\mathbf{q}}) (1 - n_{\mathbf{k}-\mathbf{q},\uparrow})] \end{aligned} \quad (\text{A9})$$

where we have only retained the imaginary part, as the real part drops out or yields an energy renormalization, which we ignore. Then, with Eq. (A1), the EOM for spin-down electron becomes

$$\frac{\partial}{\partial t} n_{\mathbf{k},\downarrow} = \frac{2\pi}{\mathcal{N}\hbar} \sum_{\mathbf{q}} M_{\text{e-m}}^2 \delta(\epsilon_{\mathbf{k}}^{\downarrow} - \epsilon_{\mathbf{k}-\mathbf{q}}^{\uparrow} - \hbar\omega_{\mathbf{q}}) [N_{\mathbf{q}} n_{\mathbf{k}-\mathbf{q},\uparrow} (1 - n_{\mathbf{k},\downarrow}) - n_{\mathbf{k},\downarrow} (1 + N_{\mathbf{q}}) (1 - n_{\mathbf{k}-\mathbf{q},\uparrow})], \quad (\text{A10})$$

for the EOM for the occupations of spin-down electrons due to electron-magnon scattering. The EOM for the occupations of spin-up electrons is obtained in the same way. The magnon distribution dynamics is derived starting

from Eq. (A2). Similar steps as in the above derivation then lead to

$$\frac{\partial}{\partial t} N_{\mathbf{q}} = \frac{2\pi}{\mathcal{N}\hbar} \sum_{\mathbf{k}} M_{\text{e-m}}^2 \delta(\epsilon_{\mathbf{k}}^{\uparrow} - \epsilon_{\mathbf{k}+\mathbf{q}}^{\downarrow} + \hbar\omega_{\mathbf{q}}) [n_{\mathbf{k}+\mathbf{q},\downarrow}(1 - n_{\mathbf{k},\uparrow})(1 + N_{\mathbf{q}}) - N_{\mathbf{q}} n_{\mathbf{k},\uparrow}(1 - n_{\mathbf{k}+\mathbf{q},\downarrow})]. \quad (\text{A11})$$

-
- [1] E. Beaurepaire, J.-C. Merle, A. Daunois, and J.-Y. Bigot, Ultrafast spin dynamics in ferromagnetic nickel, *Physical Review Letters* **76**, 4250 (1996).
 - [2] B. Koopmans, J. Ruigrok, F. Dalla Longa, and W. De Jonge, Unifying ultrafast magnetization dynamics, *Physical Review Letters* **95**, 267207 (2005).
 - [3] B. Koopmans, G. Malinowski, F. Dalla Longa, D. Steiauf, M. Fähnle, T. Roth, M. Cinchetti, and M. Aeschlimann, Explaining the paradoxical diversity of ultrafast laser-induced demagnetization, *Nature materials* **9**, 259 (2010).
 - [4] J. Walowski, G. Müller, M. Djordjevic, M. Münzenberg, M. Kläui, C. A. Vaz, and J. A. C. Bland, Energy equilibration processes of electrons, magnons, and phonons at the femtosecond time scale, *Physical Review Letters* **101**, 237401 (2008).
 - [5] D. Steiauf and M. Fähnle, Elliott-Yafet mechanism and the discussion of femtosecond magnetization dynamics, *Physical Review B* **79**, 140401 (2009).
 - [6] S. Essert and H. C. Schneider, Electron-phonon scattering dynamics in ferromagnetic metals and their influence on ultrafast demagnetization processes, *Physical Review B* **84**, 224405 (2011).
 - [7] K. Carva, M. Battiato, and P. M. Oppeneer, *Ab Initio* Investigation of the Elliott-Yafet Electron-Phonon Mechanism in Laser-Induced Ultrafast Demagnetization, *Physical Review Letters* **107**, 207201 (2011).
 - [8] Y. Yafet, g Factors and Spin-Lattice Relaxation of Conduction Electrons, in *Solid State Physics*, Vol. 14 (Elsevier, 1963) pp. 1–98.
 - [9] J. Fabian and S. Das Sarma, Spin Relaxation of Conduction Electrons in Polyvalent Metals: Theory and a Realistic Calculation, *Physical Review Letters* **81**, 5624 (1998).
 - [10] C. Grimaldi and P. Fulde, Theory of screening of the phonon-modulated spin-orbit interaction in metals, *Physical Review B* **55**, 15523 (1997).
 - [11] A. Baral, S. Vollmar, S. Kaltenborn, and H. C. Schneider, Re-examination of the Elliott–Yafet spin-relaxation mechanism, *New Journal of Physics* **18**, 023012 (2016).
 - [12] S. Vollmar, D. J. Hilton, and H. C. Schneider, Generalized Elliott-Yafet spin-relaxation time for arbitrary spin mixing, *Physical Review B* **96**, 075203 (2017).
 - [13] K. Leckron, S. Vollmar, and H. C. Schneider, Ultrafast spin-lattice relaxation in ferromagnets including spin-orbit fields, *Physical Review B* **96**, 140408(R) (2017).
 - [14] M. Krauß, T. Roth, S. Alebrand, D. Steil, M. Cinchetti, M. Aeschlimann, and H. C. Schneider, Ultrafast demagnetization of ferromagnetic transition metals: The role of the coulomb interaction, *Physical Review B* **80**, 180407 (2009).
 - [15] B. Y. Mueller, A. Baral, S. Vollmar, M. Cinchetti, M. Aeschlimann, H. C. Schneider, and B. Rethfeld, Feedback Effect during Ultrafast Demagnetization Dynamics in Ferromagnets, *Physical Review Letters* **111**, 167204 (2013).
 - [16] P. Elliott, N. Singh, K. Krieger, E. Gross, S. Sharma, and J. Dewhurst, The microscopic origin of spin-orbit mediated spin-flips, *Journal of Magnetism and Magnetic Materials* **502**, 166473 (2020).
 - [17] J. K. Dewhurst, S. Shallcross, P. Elliott, S. Eisebitt, C. von Korff Schmising, and S. Sharma, Angular momentum redistribution in laser-induced demagnetization, *Physical Review B* **104**, 054438 (2021).
 - [18] S. R. Tauchert, M. Volkov, D. Ehberger, D. Kazenwadel, M. Evers, H. Lange, A. Donges, A. Book, W. Kreuzpaintner, U. Nowak, and P. Baum, Polarized phonons carry angular momentum in ultrafast demagnetization, *Nature* **602**, 73 (2022).
 - [19] E. Carpane, E. Mancini, C. Dallera, M. Brenna, E. Puppin, and S. De Silvestri, Dynamics of electron-magnon interaction and ultrafast demagnetization in thin iron films, *Physical Review B* **78**, 174422 (2008).
 - [20] A. Manchon, Q. Li, L. Xu, and S. Zhang, Theory of laser-induced demagnetization at high temperatures, *Physical Review B* **85**, 064408 (2012).
 - [21] M. Haag, C. Illg, and M. Fähnle, Role of electron-magnon scatterings in ultrafast demagnetization, *Physical Review B* **90**, 014417 (2014).
 - [22] E. Turgut, D. Zusin, D. Legut, K. Carva, R. Knut, J. M. Shaw, C. Chen, Z. Tao, H. T. Nembach, T. J. Silva, S. Mathias, M. Aeschlimann, P. M. Oppeneer, H. C. Kapteyn, M. M. Murnane, and P. Grychtol, Stoner versus Heisenberg: Ultrafast exchange reduction and magnon generation during laser-induced demagnetization, *Physical Review B* **94**, 220408(R) (2016).
 - [23] S. Eich, M. Plötzing, M. Rollinger, S. Emmerich, R. Adam, C. Chen, H. C. Kapteyn, M. M. Murnane, L. Plucinski, D. Steil, B. Stadtmüller, M. Cinchetti, M. Aeschlimann, C. M. Schneider, and S. Mathias, Band structure evolution during the ultrafast ferromagnetic-paramagnetic phase transition in cobalt, *Science Advances* **3**, e1602094 (2017).
 - [24] C. Illg, M. Haag, and M. Fähnle, Ultrafast demagnetization after laser irradiation in transition metals: Ab initio calculations of the spin-flip electron-phonon scattering with reduced exchange splitting, *Physical Review B* **88**, 214404 (2013).
 - [25] M. Beens, R. A. Duine, and B. Koopmans, s-d model for local and nonlocal spin dynamics in laser-excited magnetic heterostructures, *Physical Review B* **102**, 054442 (2020).
 - [26] M. Beens, R. A. Duine, and B. Koopmans, Modeling ultrafast demagnetization and spin transport: The interplay of spin-polarized electrons and thermal magnons, *Physical Review B* **105**, 144420 (2022).

- [27] M. Weißenhofer and P. M. Oppeneer, Ultrafast demagnetization through femtosecond generation of non-thermal magnons, *Advanced Physics Research*, 2300103 (2024).
- [28] M. Bonitz, D. Kremp, D. Scott, R. Binder, W.-D. Kraeft, and H. S. Köhler, Numerical analysis of non-Markovian effects in charge-carrier scattering: one-time versus two-time kinetic equations, *Journal of Physics: Condensed Matter* **8**, 6057 (1996).
- [29] S. Vollmar, K. Leckron, and H. C. Schneider, Ultrafast demagnetization and its relation to microscopic momentum scattering dynamics in a rashba ferromagnet, *Phys. Rev. B* **108**, 094403 (2023).
- [30] D. M. Edwards, The paramagnetic state of itinerant electron systems with local magnetic moments. I. Static properties, *Journal of Physics F: Metal Physics* **12**, 1789 (1982).
- [31] J. Hong and D. L. Mills, Theory of the spin dependence of the inelastic mean free path of electrons in ferromagnetic metals: A model study, *Physical Review B* **59**, 13840 (1999).
- [32] V. P. Zhukov, E. V. Chulkov, and P. M. Echenique, GW + T theory of excited electron lifetimes in metals, *Physical Review B* **72**, 155109 (2005).
- [33] M. C. T. D. Müller, S. Blügel, and C. Friedrich, Electron-magnon scattering in elementary ferromagnets from first principles: Lifetime broadening and band anomalies, *Physical Review B* **100**, 045130 (2019).
- [34] J. A. Hertz and M. A. Klenin, Fluctuations in itinerant-electron paramagnets, *Physical Review B* **10**, 1084 (1974).
- [35] L. C. Davis and S. H. Liu, Electron-Magnon Interaction in Ferromagnetic Transition Metals, *Physical Review* **163**, 503 (1967).
- [36] R. M. White and R. B. Woolsey, Magnon corrections to the effective mass of an electron in a magnetic semiconductor, *Physical Review* **176**, 908 (1968).
- [37] R. B. Woolsey and R. M. White, Electron-magnon interaction in ferromagnetic semiconductors, *Physical Review B* **1**, 4474 (1970).
- [38] S. Paischer, G. Vignale, M. I. Katsnelson, A. Ernst, and P. A. Buzek, Nonlocal correlation effects due to virtual spin-flip processes in itinerant electron ferromagnets, *Physical Review B* **107**, 134410 (2023).
- [39] F. Rossi and T. Kuhn, Theory of ultrafast phenomena in photoexcited semiconductors, *Reviews of Modern Physics* **74**, 895 (2002).
- [40] M. Kira and S. W. Koch, *Semiconductor quantum optics* (Cambridge University Press, Cambridge, UK; New York, 2012).
- [41] M. Beens, J. P. Heremans, Y. Tserkovnyak, and R. A. Duine, Magnons versus electrons in thermal spin transport through metallic interfaces, *Journal of Physics D: Applied Physics* **51**, 394002 (2018), arXiv: 1804.02172.
- [42] N. H. Long, P. Mavropoulos, S. Heers, B. Zimmermann, Y. Mokrousov, and S. Blügel, Spin-flip hot spots in ultrathin films of monovalent metals: Enhancement and anisotropy of the Elliott-Yafet parameter, *Physical Review B* **88**, 144408 (2013).
- [43] K. Leckron and H. C. Schneider, Ferromagnetic model system with spin-orbit coupling: Dynamical gap and effective spin-flip scattering, *Journal of Magnetism and Magnetic Materials* **471**, 482 (2019).
- [44] M. Sakoh and D. Edwards, Magnetic properties of iron and cobalt in a combined model of itinerant electrons and localized spins, *physica status solidi (b)* **70**, 611 (1975).
- [45] R. H. Groeneveld, R. Sprik, and A. Lagendijk, Effect of a nonthermal electron distribution on the electron-phonon energy relaxation process in noble metals, *Physical Review B* **45**, 5079 (1992).
- [46] D. Mongin, P. Maioli, J. Burgin, P. Langot, E. Cottancin, S. D'addato, B. Canut, M. Treguer, A. Crut, F. Vallée, *et al.*, Ultrafast electron-lattice thermalization in copper and other noble metal nanoparticles, *Journal of Physics: Condensed Matter* **31**, 084001 (2019).
- [47] C. Voisin, N. Del Fatti, D. Christofilos, and F. Vallée, Ultrafast electron dynamics and optical nonlinearities in metal nanoparticles, *The Journal of Physical Chemistry B* **105**, 2264 (2001).
- [48] Y. Liu, L.-S. Xie, Z. Yuan, and K. Xia, Magnon-phonon relaxation in yttrium iron garnet from first principles, *Physical Review B* **96**, 174416 (2017).
- [49] B. Y. Mueller, T. Roth, M. Cinchetti, M. Aeschlimann, and B. Rethfeld, Driving force of ultrafast magnetization dynamics, *New Journal of Physics* **13**, 123010 (2011).
- [50] M. Stiehl, M. Weber, C. Seibel, J. Hofer, S. T. Weber, D. M. Nenno, H. C. Schneider, B. Rethfeld, B. Stadtmüller, and M. Aeschlimann, Role of primary and secondary processes in the ultrafast spin dynamics of nickel, *Applied Physics Letters* **120**, 062410 (2022).
- [51] H. Haug and S. W. Koch, *Quantum theory of the optical and electronic properties of semiconductors* (World Scientific Publishing Company, 2004).